HHS Public Access

Author manuscript

Oncogene. Author manuscript; available in PMC 2020 March 20.

Published in final edited form as:

Oncogene. 2020 January ; 39(3): 703–717. doi:10.1038/s41388-019-1012-2.

Inactivation of PP2A by a recurrent mutation drives resistance to MEK inhibitors

Caitlin M. O'Connor[1], **Daniel Leonard**[2], **Danica Wiredja**[3], **Rita A. Avelar**[4], **Zhizhi Wang**[5], **Daniela Schlatzer**[3], **Benjamin Bryson**[6], **Eesha Tokala**[6], **Sarah E. Taylor**[2], **Aditya Upadhyay**[6], **Jaya Sangodkar**[7], **Anne-Claude Gingras**[8], **Jukka Westermarck**[9], **Wenqing Xu**[5], **Analisa DiFeo**[4], **David L. Brautigan**[10], **Shozeb Haider**[11], **Mark Jackson**[6], **Goutham Narla**[7]

[1]Department of Pharmacology, Case Western Reserve University, Cleveland, OH, USA. [2]Department of Pathology, Case Western Reserve University, Cleveland, OH, USA. [3]Department of Proteomics and Bioinformatics, Case Western Reserve University, Cleveland, OH, USA. [4]Department of Pathology, University of Michigan, Ann Arbor, MI, USA. [5]Department of Biological Structure, University of Washington, Seattle, WA, USA. [6]Case Comprehensive Cancer Center, Case Western Reserve University, Cleveland, OH, USA. [7]Department of Internal Medicine: Genetic Medicine, University of Michigan, Ann Arbor, MI, USA. [8]Lunenfeld-Tanenbaum Research Institute, Sinai Health System, Toronto, ON, Canada; Department of Molecular Genetics, University of Toronto, Toronto, ON, Canada. [9]Turku Centre for Biotechnology, University of Turku and Åbo Akademi University, Turku, Finland. [10]Department of Microbiology, Immunology, and Cancer Biology, University of Virginia, Charlottesville, VA, USA [11]Department of Pharmaceutical and Biological Chemistry, University College London, London, United Kingdom

Abstract

The serine/threonine Protein Phosphatase 2A (PP2A) functions as a tumor suppressor by negatively regulating multiple oncogenic signaling pathways. The canonical PP2A holoenzyme is comprised of a scaffolding subunit (PP2A Aα/β), which serves as the platform for binding of both the catalytic C subunit and one regulatory B subunit. Somatic heterozygous missense mutations in *PPP2R1A*, the gene encoding the PP2A Aα scaffolding subunit, have been identified across multiple cancer types, but the effects of the most commonly mutated residue, Arg-183, on PP2A function have yet to be fully elucidated. In this study, we used a series of cellular and *in vivo* models and discovered that the most frequent Aα R183W mutation formed alternative holoenzymes by binding of different PP2A regulatory subunits compared to wild type Aα,

To whom correspondence should be addressed: Goutham Narla, gnarla@med.umich.edu.

Author Contributions

CMO and GN designed the research studies. CMO wrote the manuscript and GN edited the manuscript. CMO, DL, DW, RA, ZW, DS, BB, ET, AU, ST, and SH performed experiments and interpreted the data. JS, A-CG, JW, WX, AD, DB, SH, MJ, and GN provided observations and scientific interpretations. All authors discussed results and provided input on the manuscript.

Conflict of Interest Statement: The authors declare no potential conflicts of interest.

Study Approval

All animal experiments were approved by the Institutional Animal Care and Use Committee (IACUC) at Case Western Reserve University. Animal use and care was in strict compliance with institutional guidelines and all experiments conformed to the relevant regulatory standards established by Case Western Reserve University.

suggesting a rededication of PP2A functions. Unlike wild type Aα, which suppressed tumorigenesis, the R183W mutant failed to suppress tumor growth *in vivo* through activation of the MAPK pathway in RAS-mutant transformed cells. Furthermore, cells expressing R183W were less sensitive to MEK inhibitors. Taken together, our results demonstrate that the R183W mutation in PP2A Aα scaffold abrogates the tumor suppressive actions of PP2A, thereby potentiating oncogenic signaling and reducing drug sensitivity of RAS-mutant cells.

Keywords

PP2A; PPP2R1A; RAS; AZD-6244; drug resistance

Introduction

The serine/threonine Protein Phosphatase 2A (PP2A) functions as a tumor suppressor by negatively regulating multiple oncogenic signaling pathways, particularly RAS driven signaling[1,2]. Importantly, PP2A inactivation is necessary to fully transform RAS expressing human epithelial cells, and PP2A and RAS have been shown to regulate overlapping signaling pathways, highlighting the cooperation between these two proteins in maintaining balanced cellular signaling[3-5]. In further support of this, the activation of PP2A has been shown to inhibit RAS-driven tumor growth in multiple cell types[6,7]. PP2A dysregulation in human cancer occurs through multiple mechanisms, including increased expression of endogenous PP2A inhibitor proteins and somatic mutation[8]. The canonical PP2A holoenzyme is comprised of a scaffolding subunit (PP2A Aα/β), which serves as the platform for binding of both the catalytic subunit (PP2A Cα/β) and one regulatory B subunit, from a distinct set of family members of B's (e.g. B55, B56, B72), which direct PP2A substrate specificity[9,10]. The PP2A A subunit exists as two isoforms, α and β, and while they share 86% sequence homology they have been suggested to act as functionally distinct proteins[4,11]. The scaffolding subunit Aα is a flexible protein comprised of 15 tandem HEAT (Huntington, Elongation factor 3, A-subunit, TOR) repeats[12]. Of these repeats, HEAT 2-8 contact with the regulatory subunits and HEAT 11-15 with the PP2A C subunit.

Heterozygous mutations to the PP2A Aα subunit are the most common mutations among all PP2A subunits, occur in multiple cancer subtypes, and have been shown to alter holoenzyme formation and regulatory B subunit binding[13-16]. The Aα E64D and R418W mutations were shown to result in functional haploinsufficiency through activation of the PI3K/AKT pathway[17]. In two independent mouse models, E64D knock-in mice had increased incidence of benzopyrene-induced lung cancer or decreased survival when crossed to $KRAS^{G13D}$ mice[18,19]. Additionally, characterization of recurrent Aα mutations in endometrial cancer has shown that the S256F mutation functions in a dominant negative manner through association with the PP2A inhibitor TIPRL and the W257G mutation increased cell migration[16,20].

Previous reports have focused on understanding the function of recurrent Aα mutations in models of endometrial cancer, and while mutational rates to Aα are highest in this context,

mutations occur across all cancer types. To explore the mechanism by which recurrent Aα mutations contribute to cancer progression, we focused our studies on the most common mutation, R183W, which occurs in multiple cellular contexts. Previous studies have only studied this mutation in endometrial cancer and have analyzed the binding of a few specific regulatory subunits[16,20]. Importantly, the effects of the R183W mutation on the global Aα interactome, oncogenic signaling, and *in vivo* tumor growth have not previously been reported.

Here we show that expression of this mutation in a mammary model of transformation and a colon cancer cell line resulted in loss of PP2A tumor suppressive activity, indicating enhanced oncogenic signaling. Biophysical studies demonstrated that R183W caused significant structural changes in the Aα protein resulting in altered PP2A activity through reduced catalytic activity, the loss of interaction with tumor suppressive PP2A B regulatory subunits, and the gain of association with Striatin subunits. Global phosphoproteomic profiling of R183W expressing cells revealed activation of the MAPK pathway, subsequently confirmed by western blotting. Accompanying these changes, R183W expressing cells were less sensitive to MEK inhibitors. Combined, our data suggests a mechanism by which the most common PP2A mutation in human cancer potentiates RAS signaling and decreases sensitivity to MEK inhibitors.

Methods

Cell Lines and Treatment.

Human cancer cell lines, SW620, H358, and H293T, were purchased from ATCC, UT89 was generated from a primary recurrent uterine serous tumor in the laboratory of Dr. Analisa DiFeo. SW620 and H358 were cultured in RPMI, H293T and UT89 were cultured in DMEM. All media was supplemented with 10% FBS (ThermoFisher, SH3007003) and 1% penicillin/streptomycin (GE Healthcare, SV30010). HMECs were obtained from Dr. Mark Jackson. Specimen 48R and derivatives were grown as described previously[21,22]. HMEC derivatives were generated as previously described[21,23]. All cells were grown in a humidified atmosphere containing 5% CO_2. All cells lines underwent monthly testing for mycoplasma contamination (Lonza, LT07-710). AZD-6244 (Selleck Chemical, S1008) was dissolved in DMSO at a concentration of 80 mM and stored at −20°C (for *in vitro* studies). Okadaic Acid (OA) (P212121, LC-O-2220) was dissolved in DMSO at a concentration of 10 mM and stored at −20°C.

Clonogenic Assays.

500 HMEC M/R cells were plated in 6-well plates and grown for 10 days. For treatment studies, cells were treated with vehicle (DMSO) or AZD-6244 for 10 days. Colonies were fixed in a solution of 10% acetic acid and 10% methanol, stained with crystal violet (1% crystal violet in methanol), and counted using ImageJ.

Constructs and Mutagenesis.

Gateway V5-tagged lentiviral expression vector pLX304-PP2A-Aα was obtained by DNASU Plasmid Repository (HsCD00444402) deposited by The ORFeome

Collaboration[24]. pLX304-PP2A-Aα was sequence verified to be wild type. pLX304-EGFP was created by Gateway cloning EGFP into pLX304 vector. pLX304-PP2A-Aα-R183W was generated by site directed mutagenesis (Agilent, 210513). After cloning and mutagenesis all constructs were sequence verified by Sanger sequencing. pLKO shRNA constructs for B56β, B56γ, Striatin, and Striatin 3 were gifts from Dr. Alejandro Gutierrez.

Virus Production and Infection.

Lentiviruses were packaged in 293T cells using X-tremeGENE transfection reagent (Sigma, 63666244001) and the second-generation packaging constructs pMD2.G (Addgene, 12259) and psPAX2 (Addgene, 12260). Supernatant media containing virus was collected at 24-48 hours and supplemented with 4 μg/mL polybrene (Santa Cruz, sc-134220). Cells were transduced for 24 hours and cultured for 48 hours before being selected with 4 μg/mL (HMEC cell lines) or 16 μg/mL of Blasticidin (SW620, H358 and UT89) (Invivogen, ant-bl-5b).

Immunoblot Analysis.

Whole cell extracts were prepared by incubating cell pellets in RIPA lysis buffer (ThermoFisher, P189901). Tumor extracts were prepared by mechanical homogenization of tissue in TPER tissue protein extraction reagent (ThermoFisher, 78510). All lysis buffers were supplemented with protease and phosphatase inhibitors (Roche, 05892791 & 09406837). Protein concentrations of cell extracts was determined by Pierce BCA Protein Assay (ThermoFisher, 23250) and equal quantities of protein were separated by SDS/PAGE 12% polyacrylamide gels (Bio-Rad, 456-8045) and transferred to nitrocellulose membranes (Bio-Rad, 1704158). Primary antibodies used in this study can be found in Table S2. Primary antibodies were detected with goat anti-mouse obtained from Abcam (ab131368) or donkey anti-rabbit conjugated to horseradish peroxidase obtained from GE Healthcare (NA934), using the Bio-Rad ChemiDoc XRS chemiluminescence imager. Densitometry quantification was performed within the Bio-Rad Image Lab software.

V5 Affinity Purification-Mass Spectrometry (AP-MS) and Co-Immunoprecipitation Analysis.

SW620, HMEC, H358, and OV89 stable cell lines were plated to 70% confluency in 150 mm plates. After 24 hours, cells were harvested and co-immunoprecipitation was performed per Dyna-beads Co-Immunoprecipitation protocol (ThermoFisher, 14321D). V5 antibody (Abcam, ab27671) was coupled at a concentration of 7 μg/mg of Dyna-beads. Following incubation of the antibody-coupled Dyna-beads with cell lysate, half of the beads were reserved for mass spectrometry analysis and the remaining half was eluted for Immunoblot analysis. Digestion for AP-MS samples were performed using an on-bead digestion protocol. Briefly, magnetic beads were washed 3 times with 100mM Tris-EDTA (pH 8) and supernatant removed. Thirty microliters of 100mM Tris-EDTA (pH 8) was added to beads. Bead-bound proteins were reduced with 10mM dithiothreitol for 1-hour at 37°C, followed by alkylation with 25mM iodoacetaminde for 30min in the dark. After reduction/alkylation of proteins a dual digestion was performed with 0.3 micrograms of lysyl endopeptidase on a dry bath shaker for 1 hour at 37°C followed by the addition of 0.3 micrograms of trypsin with incubation overnight at 37°C. After digestion, samples were filtered with 0.22μM spin filters to remove any particulates prior to MS analysis (Costar Spin-X, Sigma-Aldrich).

Peptides were sequenced using data dependent MS acquisition (DDA) as previously described [25]. Fresh conjugated beads were prepared for each biological replicate, three biological replicates were performed for each experiment.

AP-MS Interaction Scoring and Data Visualization.

SAINTexpress AP-MS software, accessible through the CRAPome, was used to filter and score interactions using three replicates of EGFP-V5 (per cell line) as a negative control[26,27]. Default SAINT express options were utilized. SAINTexpress files were uploaded to ProHits-viz for data visualization and dot plot generation[28]. The default ProHits-viz options were *primary filter* = 0.01 and *secondary filter* = 0.05 (corresponding to FDR), with a *minimum abundance value* = 0 and a *maximum abundance value* = 50. No normalization or log transformation was utilized for data visualization.

Phosphatase Activity Assay.

HMEC M/R stable cell lines were plated to 70% confluency in 150 mm plates. After 24 hours, cells were lysed in phosphatase buffer consisting of 25 mM HEPES, 1 mM MgCl, 0.1 mM MnCl, 1% Triton-X, and protease inhibitor. 5 mg of protein lysate was incubated with 1.5 mg of V5-antibody conjugated beads (described above) and incubated on a roller for 30 min at 4°C. Beads were washed 3X with phosphatase assay buffer consisting of 25 mM HEPES, 1 mM MgCl, and 0.1 mM MnCl. Following washes, an aliquot of the beads was reserved for Western blotting. For the phosphatase assay, the remaining beads were resuspended in phosphatase assay buffer supplemented with 1 mM DTT (100 μL/1 mg) and incubated with increasing concentrations of DiFMUP (ThermoFisher, D6567) on a shaker for 15 min at 37°C. Fluorescence was measured at 365/455 nm. Measurements taken from V5-EGFP expressing cells were used to subtract background. Rate of phosphatase activity was calculated by fluorescent units divided by the incubation time (fluorescent units/min). Final activity was normalized to the total PP2A C subunit levels in the IP material determined by Western blot.

Xenograft Tumor Formation and AZD-6244 Treatment Studies.

5×10^6 SW620 cells were injected subcutaneously in 50% matrigel into the right flanks of 6-8-week-old female Balb/c *nu/nu* mice. Tumors were allowed to grow to 100 mm^3, then randomized into control or AZD-6244 (25 mg/kg BID) treatment groups and tumor volume was assessed by caliper measurement every other day. No blinding was performed. In each experiment, the minimum number of animals is utilized to establish the validity and reproducibility of the results. Ten animals per treatment group are required to establish a statistical difference between groups and to ensure enough animals remain throughout the observation time period accounting for unexpected deaths or morbidity unrelated to the experiment. These numbers have been empirically determined in previous experiments within the lab as necessary in order to observe and calculate statistical differences between experimental and control groups of animals. Assuming a sigma of 0.3, 10 mice/group should achieve 80% power to detect a ≥40% difference in tumor volume (two-sample t-test power analysis). Tumor tissue was harvested two hours after the final dose of the treatment study. Tumor tissue was both formalin-fixed, for IHC, and snap frozen in liquid nitrogen for

immunoblotting and phosphoproteomics analysis. For *in vivo* treatment studies, AZD-6244 was dissolved in 10% DMA, 10% solutol, and water.

Phosphoproteomics.

Sections from three tumors representative of the average tumor growth of each group from the SW620 xenograft were utilized for phosphoproteomic analysis. Tissue was rinsed with 1xPBS to remove any residual blood contaminated prior to sample preparation. Tissue was subsequently solubilized with 2% Sodium dodecyl sulfate (SDS) containing protease and phosphatase inhibitors. Detergent removal was performed using the FASP cleaning procedure and eight hundred micrograms of each sample was digested enzymatically with a two-step LysC/trypsin digestion[29]. Phosphopeptides were enriched with titanium dioxide and analyzed by LC-MS/MS using a UPLC system (NanoAcquity, Waters) that was interfaced to Orbitrap ProVelos Elite mass spectrometer (Thermo Fisher) and quantified as previously described[30].

KSEA and Pathway Analysis.

KSEA analysis was based on the approach originally described by Casado *et al.* and executed with the "KSEAapp" R package version 0.99.0, available through the CRAN repository, with the NetworKIN = FALSE feature applied[31,32]. Pathway analysis was performed at the protein level using the Reactome database of pathways[33]. Each protein was represented by the phosphopeptide with the most significant one-way ANOVA p-value across all the groups. One-sided Fisher's exact test was used to calculate the pathway enrichment of proteins that have a log2(fold change) of (A) 1.5 or greater for enrichment of hyper-phosphorylated* proteins or (B) −1.5 or lower for enrichment of dephosphorylated* proteins. Fold change was calculated relative to EGFP. All calculations and related plots were performed/generated in R version 3.3.2. *Due to the absence of a total protein arm in the phosphoproteomics experiment, we cannot confirm if each protein's abundance is altered amongst the different conditions; thus, the "hyper-phosphorylated" and "dephosphorylated" terms are used with the assumption that there is no underlying change in the total protein level between the two compared conditions.

Molecular Dynamics Simulations.

Structural coordinates of PP2A were downloaded from the PDB. (ID 2IAE). The R183W mutant was constructed *in silico* using the ICM mutagenesis software[34]. The systems were prepared for simulations using the High-throughput Molecular Dynamics (HTMD) package[35]. The systems were defined using Amber99SB14 force field, employing explicit TIP3P water molecules as solvent[36,37]. The systems were minimized with 1000 steps of steepest descent integrator and equilibrated in the NPT ensemble for 5 ns, using a Berendsen barostat at 1 atm[38]. The temperature was kept at 300 K° by a Langevin thermostat. A 1050 ns production run was carried out for all the systems in the NVT ensemble with a time step of 4 fs. All the simulations were carried out with the ACEMD program[39]. Well-Tempered Metadynamics (WTMetaD) of the A subunit wild-type and mutant structure was performed at 300 K using the software ACEMD and the PLUMED plugin using an integration step of 4 fs[40]. To study the influence of R183 and R183W mutant on the conformation of the A subunit, we chose the dihedral angles of the WT/mutated residue to be the collective variable

(CV). The choice of the CVs (CV1 = phi and CV2 = psi) was based on the observation that the slowest motions in a protein are a function of their backbone flexibility[41]. Therefore, the differences in the structural effects resulting from the changes between wild-type and the mutant should be pronounced in the dihedral angles. A total of 450 ns in the NVT ensemble were needed to reach full convergence of the free energy. The free energy surface of the WTMetaD simulation as a function of the two CVs is readily obtained by integrating the deposited energy bias along the trajectory. The error on the minima and barriers of the free energy surface was estimated from the largest variation observed in the mono-dimensional projections along the collective variables during the last 100 ns of the simulation. It amounts to 0.5 kcal/mol.

The structures corresponding to the minima were selected from the WTMetaD trajectories, based on the values of collective variables CV1 and CV2 using analysis tool of the GROMACS package[42]. The structural figures were generated using VMD, ICM-Pro and PyMol softwares[34,43,44].

Results

R183 is the most commonly mutated residue of PP2A Aα

In human tumors, 374 heterozygous missense mutations have been identified in the PP2A Aα subunit (as of June 2018 from cBioPortal.org). The overall somatic mutation frequency to Aα across all cancers is approximately 1%, and interestingly, the distribution of mutations in the PP2A scaffold subunit is nonrandom, resulting in a mutational hotspot within HEAT 5 of the protein (Figure 1A)[13,14,45-47]. The most commonly mutated residue to the Aα scaffolding protein is Arg-183, and mutation to this residue results in either a tryptophan (R183W) or a glutamine (R183Q) at this position, with tryptophan (R183W) occurring most frequently (Figure 1A). Mutation to a glycine (R183G), has been reported in smaller sequencing cohorts, but has not been identified in larger whole genome sequencing efforts[14,48]. Arg-183 mutations are recurrent in multiple cancer types, with the majority of these found in colorectal (CRC), uterine, and breast cancers (Figure 1B).

Aα R183W alters the PP2A interactome and protein conformation

PP2A inactivation has been shown to fully transform human epithelial cells expressing RAS[5]. Additionally, analysis of sequencing data available on cBioPortal revealed that the R183W mutation coexists with KRAS mutations at a significant frequency in patient tumors (Supplemental Figure 1). To evaluate the relevance of the PP2A Aα R183W mutation in RAS driven models, we used the KRAS mutant colorectal cancer cell line SW620 as well as a RAS dependent human mammary epithelial cell (HMEC) model of transformation, shp16-shp53-Myc/RAS cells (M/R), described previously[21]. We stably expressed V5-tagged WT or R183W Aα into the transformed shp16-shp53-Myc/RAS cells (M/R) and SW620 cells using a lentiviral approach. Given that studies have shown that PP2A Aα mutations result in altered holoenzyme complex formation and Aα interactome[16,19,20], we first used co-immunoprecipitation of V5-tagged WT or R183W Aα protein in our cell models, SW620 and M/R cells, followed by mass spectrometry analysis (AP-MS) to determine the effect of the R183W Aα mutation on global protein interactions, and confirmed select changes by

immunoblotting (Figure 2, A-E and Supplemental Figure 2, A and B). Consistent with published literature, the R183W mutation lost the majority of B56 (B'), B55 (B) and B" family member binding, while also resulting in an increased binding to Striatin family members (B'") (Figure 2 A-E, Supplemental Figure 2C). Beyond impacting the binding of PP2A subunits, mass spectrometry analysis identified differential binding of additional proteins, including STRIPAK components and members of the Integrator Complex (Figure 2A). Additionally, the R183W mutation did not have a significant impact on C subunit binding when the co-immunoprecipitation was quantified by mass spectrometry (Figure 2A) or by immunoblot following co-immunoprecipitation (Figure 2C and D). These changes to the Aα interactome were consistent in two additional cell lines, H358 (non-small cell lung cancer) and UT89 (primary uterine serous cancer) (Supplemental Figure 3, A-C). We performed a binding assay in a cell free system with recombinant A/C dimer and B56α. Incubation of recombinant wild type or mutant R183W A/C with B56α tagged beads confirmed the R183W mutant A/C dimer fails to bind B56α *in vitro* (Supplemental Figure 2C). To determine the effects of the R183W mutation on PP2A activity, we performed phosphatase activity assays using DiFMUP on co-immunoprecipitated lysates from WT and mutant R183W Aα expressing M/R cell lines (Figure 2F and Supplemental Figure 4, A-D). We calculated Michaelis-Menten kinetics for the WT and mutant R183W Aα protein, revealing that while K_m was relatively unchanged with the R183W mutation, V_{max} was substantially decreased. This indicated that while the R183W Aα mutation did not affect the affinity of DiFMUP for PP2A, the maximal rate of catalysis was reduced (Figure 2F and Supplemental Figure 4E). To determine if the interactome differences were a result of localization changes between the wild type and mutant Aα proteins, we performed cytosolic and nuclear fractionation of cell lysates from WT or R183W expressing M/R cells. Following fractionation, we performed western blot analysis of select PP2A subunits, and found that localization of all subunits was unaffected by the R183W mutation, indicating that the interactome changes were not due to compartmentalization changes of the Aα scaffold itself or its interacting regulatory subunits (Figure 2G). The striking differences in the interactome and the activity of the WT and R183W Aα proteins led us to investigate the possible structural explanations for these differences. We performed molecular dynamics simulations of WT and R183W Aα to identify stable protein conformations. The free energy landscape plots were generated as a function of ϕ and ψ dihedral angles of the residues R183 and the mutant R183W (Figure 2, H and I, Supplemental Figures 5-7). These landscapes provide evidence that the R183W mutant is capable of exploring an altered free energy landscape to adopt multiple metastable conformations of the Aα subunit, which may alter interactions with other proteins. Using these landscapes, we extracted conformations from the most stable conformation of the WT and R183W mutant protein, designated with an "A/B" (Figure 2, H and I). These conformations indicate that R183 makes multiple interactions with N211 in the wild type Aα protein, which is facilitated by an ion pair interaction between R182 and D215. These interactions are all lost when mutated to a tryptophan. Together, these data show that the R183W mutation to the Aα scaffold protein disrupts protein conformation and in turn alters the interactome of this protein.

Introduction of the Aα R183W mutation loses growth suppressive phenotype in M/R cells and SW620 tumors

Interference of PP2A functions, through altered expression of select subunits or through the expression of SV40 ST antigen, results in cellular transformation[3,5,49]. To assess the functional role of the recurrent R183W Aα mutation on cell growth, we stably expressed V5-tagged WT or R183W Aα into the transformed shp16-shp53-Myc/RAS cells (M/R) or SW620 cells using a lentiviral approach (Figure 3A and 3B). Importantly, consistent with previous literature, the stability and expression of the C subunit is closely linked to the expression of the A subunit (Figure 3B)[50-52]. Clonogenic assays in the M/R cells showed that expression of WT Aα significantly decreased the ability of these cells to form 2D colonies, while R183W Aα did not maintain these growth suppressive effects (Figure 3C). To test the oncogenic potential of R183W Aα mutant expressing SW620 cells, we injected these stable isogenic cell lines into a subcutaneous xenograft model of tumorigenesis. While WT Aα overexpression resulted in reduced tumor growth *in vivo*, the expression of R183W Aα mutant did not mimic this growth suppressive effect (Figure 3D). In both models, expression of R183W in cells or tumors caused no growth changes and behaved similarly to the EGFP controls (Figure 3C and D). Taken together, our cellular and *in vivo* models suggest that additional expression of WT Aα increases PP2A's tumor suppressive function and results in a growth suppressive phenotype which is lost when the R183W mutation is introduced, indicating that the R183W mutation may be loss of function in this context.

Expression of R183W potentiates MAPK signaling in KRAS mutant cells

To determine the impact of the R183W Aα mutant on oncogenic signaling, we performed global serine/threonine phosphoproteomics on three tumors which were representative of the average tumor growth for each independent group from the SW620 xenograft study (Figure 3D). Overall, we identified and quantified 3860 peptides mapping to 3206 phosphoproteins. To analyze the phosphoproteomic data set, we utilized Kinase Substrate Enrichment Analysis (KSEA)[31,32]. KSEA uses known kinase-substrate relationships and calculates the potential kinase activity based on the phosphorylation levels of its known substrates. In our data set, this analysis showed an alteration in signaling output of multiple kinases (Figure 4A and Supplemental Figure 8). The most significantly altered kinase identified was MAP2K1, or MEK, the kinase responsible for phosphorylating ERK1/2 at T202/Y204. Additionally, MAP2K1 was one of only two kinases shown to be altered when the phosphorylation levels in R183W Aα tumors were compared to both WT Aα and EGFP (Figure 4A). This finding was subsequently confirmed by western blot, where expression of R183W Aα resulted in a significant increase in p-ERK levels when compared to either WT Aα or control vector expressing tumors (Figure 4B-D). In support of this finding, pathway analysis of significantly hyper phosphorylated peptides from the phosphoproteomics results showed enrichment for MAPK/ERK related pathways in the R183W expressing tumors compared to control vector (Supplemental Figure 9). To determine the effects of the R183W mutant on oncogenic RAS signaling in the HMEC model of transformation, we performed phospho-specific immunoblotting on p-ERK (T202/Y204) in the isogenic M/R cells. We found significantly increased phosphorylation of p-ERK (T202/Y204) in cells expressing the R183W mutant Aα compared to WT cells (Figure 4E and F). To determine if the observed increase in p-ERK (T202/Y204) levels in the R183W expressing cells were a result of

decreased PP2A catalytic activity, we treated the control M/R cells with 250 nM of okadaic acid (OA), a PP2A inhibitor, for 1 hour. Following treatment, we measured p-ERK levels by western blot and found that OA treatment in this cell model significantly increased phosphorylation of p-ERK (T202/Y204), indicating that the decreased catalytic activity in this mutant could be contributing to the observed increases in p-ERK expression (Figure 4G and H).

Phosphorylation of ERK at T202/Y204 has been shown to be both negatively (including, but not limited to the B56β and B56γ regulatory subunits) and positively regulated (through the Striatin and Striatin 3 regulatory subunits) by PP2A[53,54]. Interestingly, the R183W mutant resulted in a loss of B56 family subunit binding and an increase in Striatin family subunit binding (Figure 2A). To determine if the observed increase in p-ERK (T202/Y204) in the mutant expressing cells and tumors was due to the interactome changes of these regulatory subunits, we transiently knocked down B56β and B56γ in M/R +WT cells or Striatin and Striatin 3 in M/R +R183W cells (Figure 4I-L, Supplemental Figure 10). In these experiments, we observed no significant changes in p-ERK (T202/Y204) levels upon transient knockdown of B56β and B56γ in the M/R +WT cells, indicating that the loss of binding of these regulatory subunits to the R183W mutant was not contributing to the observed increase in p-ERK expression (Figure 4I and J). However, there was a significant increase in p-ERK levels upon knockdown of Striatin in the M/R +R183W cells (Figure 4K and L). Interestingly, upon knockdown of Striatin or Striatin 3, there was a compensatory increase in the other Striatin (Figure 4K, Supplemental Figure 10). Additionally, the increase in Striatin 3 expression also correlated with an increase in V5 expression of the R183W mutant, consistent with published literature that certain Aα mutants' expression is linked to Striatin 3 expression[16]. Combined, this may suggest that stabilization of the inactive R183W mutation, through the increase in Striatin 3 expression, further increased p-ERK expression in this model (Figure 4K and L). Interestingly, mutation to the R183 residue most often occurs in colorectal cancer, in which 20-30% of patients have KRAS mutations, and in the identified CRC harboring R183 mutations, 57% had KRAS mutations (Supplemental Table 1), indicating that R183 mutations may co-occur with KRAS mutations in CRC. Taken together, this data confirms the hyper-phosphorylation of ERK upon expression of the R183W *in vitro* and *in vivo* and suggests that inactivation of PP2A by the mutant R183W Aα cooperates with the oncogene RAS to potentiate MAPK signaling.

Expression of Aα R183W decreases sensitivity to MEK inhibitors

Our results in M/R and SW620 cells indicated that expression of R183W increased MAPK signaling. Additionally, it has been shown recently that inactivation of PP2A through siRNA-mediated silencing of the A subunit results in MEK inhibitor resistance[7]. To determine if the increase in MAPK signaling impacted response to therapy, we treated M/R cells with a MEK inhibitor, AZD-6244, in a colony formation assay. M/R cells expressing Aα R183W were less sensitive to MEK inhibition than the parental M/R cells or cells expressing WT Aα (Figure 5A-C). Interestingly, the expression of WT Aα increased the sensitivity to MEK inhibition, suggesting that increased PP2A phosphatase activity may enhance the efficacy of kinase inhibitors (Figure 5 A-C). To determine if these effects were consistent with an *in vivo* model, we treated SW620 tumors with AZD-6244 (Figure 5D).

Although all tumors responded to AZD-6244, after 22 days of treatment, tumors expressing R183W had a significantly larger tumor volume than vector control tumors, while tumors expressing WT were not significantly different than vector control tumors (Figure 5D and Supplemental Figure 11). In the SW620 xenograft model, over expression of WT Aα did not sensitize tumors to AZD-6244, as was seen in the M/R-WT cell lines by 2D colony formation.

Intrinsic resistance to MEK inhibitors has been in part attributed to MEK-ERK reactivation and the activation of parallel oncogenic pathways. AZD-6244 treatment decreased phosphorylated ERK induced by Aα R183W, both in the SW620 xenograft and in M/R cells (Supplemental Figure 11 and 12). Treatment with AZD-6244 resulted in increases in phosphorylation of MEK in both WT and R183W Aα expressing cells and tumors, indicating that MEK-ERK reactivation was not a resistance mechanism in this model (Supplemental Figure 11 and 12). Compensatory activation of PI3K/AKT/mTOR signaling has been implicated in MEK inhibitor resistance and the dual inhibition of AKT or mTOR and MEK has been shown to enhance apoptosis and tumor growth suppression[55,56]. Given the baseline alterations in AKT signaling detected in the phosphoproteomics KSEA analysis (Figure 4B), we measured phosphorylation levels of the AKT pathway in AZD-6244 treated M/R cells expressing WT or R183W Aα. Interestingly, the baseline levels of phosphorylated AKT (S473) were significantly lower in the M/R cells expressing R183W Aα (Supplemental Figure 12). Upon inhibition of MEK by AZD-6244, the phosphorylation levels of AKT returned to the baseline levels seen in the control or M/R cells expressing WT Aα. Taken together, our data suggest that expression of R183W Aα decreased the sensitivity of cells and tumors to the MEK inhibitor AZD-6244 and the identified MEK inhibitor resistance mechanism was not mediated through the upregulation of MEK-ERK pathway or robust upregulation of the parallel AKT signaling pathway, suggesting that other PP2A-dependent pathways could be involved in MEK inhibitor resistance.

Discussion

The goal of this study was to elucidate the functional role and potential clinical relevance of the PP2A Aα R183W mutant in tumorigenesis and response to therapy. Here, we demonstrate that this recurrent PP2A mutation may enhance tumorigenesis through the loss of key tumor suppressive regulatory subunits resulting in potentiation of RAS signaling and decreased sensitivity to MEK inhibitors.

Our co-immunoprecipitation assays in several different cellular contexts revealed interaction changes to Aα which were conserved across all cell types studied. Despite significantly reduced PP2A catalytic activity, significant changes in PP2A C binding to the R183W mutant were not seen in any cellular context. The R183W mutation also dramatically reduced binding to the majority of the B55, B56 and PR72/PR130 subunit family members. Through molecular modeling we showed a marked conformational change in the R183W mutant Aα protein, suggesting that the altered PP2A catalysis and loss of regulatory subunit binding could be, in part, through altered protein conformation. This may be explained by work showing the dynamic and elastic nature of the A subunit can influence catalysis by altering the distance of the B/C interface as well as the orientation of the catalytic residues

within the C subunit[57,58]. Further, it has been proposed that partial unfolding of the A subunit may enhance subunit binding, utilizing a "fly-casting mechanism"[58]. Future analysis of the R183W mutant protein and how it may impact the dynamic nature of protein folding may help explain the disruption in regulatory subunit and other protein binding partners. Additionally, some of the interaction changes caused by the R183W mutation were context-dependent. For example, a gain in binding of the components of the integrator complex was only detected in the CRC cell line SW620. These context-dependent changes could be associated with the expression of certain proteins within a particular histological subtype and further exploration would be useful in understanding the histological distribution of the R183W mutation at varying frequencies across different cancer types.

The study of the effects of PP2A Aα subunit mutations on signaling has been limited to analysis of known direct PP2A targets, and the analysis of phosphorylation changes at a global level has remained unexplored. Here, we utilized global phosphoproteomics and subsequent bioinformatics analysis to provide a more comprehensive picture of the pathways and proteins altered upon mutation of *PPP2R1A*. Given the broad biological role of PP2A holoenzymes in cellular signaling cascades, it is unsurprising that a mutation to the common scaffolding subunit would have such broad effects in the phosphoproteome. Additionally, these results suggest the potential role of oncogenic drivers and histological context to affect signaling as the increased ERK phosphorylation and decreased AKT phosphorylation identified in the colorectal SW620 and mammary M/R cells expressing R183W are different than those seen with Aα mutations in endometrial cancers[16].

Targeting of the ERK-RAS pathway through inhibition of MEK1/2 has been shown to be a promising therapeutic approach in certain cancer subtypes; however, resistance and feedback mechanisms have limited the overall clinical benefit. These resistance mechanisms include parallel pathway activation in response to MEK inhibition, reactivation of the MEK-ERK pathway, and adaptive kinome reprogramming[59]. Our findings show that the R183W Aα mutation works in part by potentiating oncogenic RAS signaling, which results in the upregulation of ERK pathway signaling and a decreased sensitivity to MEK inhibitors. However, the identified MEK inhibitor resistance mechanism was not mediated through the upregulation of MEK-ERK pathway or robust upregulation of the parallel AKT signaling pathway, suggesting that other PP2A-dependent pathways could be involved in MEK inhibitor resistance. Tumors expressing mutant R183W Aα displayed a global altered phosphoproteome, indicating that the R183W mutant may result in signal re-wiring via multiple mechanisms, including loss or gain of regulatory subunit binding and altered PP2A activity, read out as decreased MEK inhibitor sensitivity. The specifics of this re-wiring and their impact on targeted cancer therapeutics are an area of further investigation.

In summary, we show cellular, *in vivo*, and structural evidence that the recurrent PP2A Aα mutation, R183W, may enhance tumorigenesis through the loss of key tumor suppressive regulatory subunits and altered PP2A catalytic activity, thereby potentiating oncogenic RAS signaling. In addition, we show that although this recurrent mutation potentiates RAS signaling, these cells were less responsive to MEK inhibition, supporting that mutation to Aα, in particular R183W, could be predictive of MEK inhibitor response.

Supplementary Material

Refer to Web version on PubMed Central for supplementary material.

Acknowledgements

The authors wish to acknowledge the Young Scientist Foundation and the students who worked on this project through this program, including Aditya Upadhyay. This work was partially supported by the NIH/NCI R01CA181654 (to GN) and T32GM008803 (to CMO). This publication was made possible in part by the Clinical and Translational Science Collaborative of Cleveland, 4UL1TR000439 from the National Center for Advancing Translational Sciences (NCATS) component of the National Institutes of Health and NIH roadmap for Medical Research. This research was supported by the Athymic Animal and Preclinical Therapeutics and Cytometry & Imaging Microscopy cores of the Case Comprehensive Cancer Center at Case Western Reserve University (funded by NIH P30 CA043703). G. Narla is supported by the Pardee-Gerstacker Professorship in Cancer Research.

References:

1. Kauko O et al. Label-free quantitative phosphoproteomics with novel pairwise abundance normalization reveals synergistic RAS and CIP2A signaling. Scientific reports 5, 13099, doi: 10.1038/srep13099 (2015). [PubMed: 26278961]
2. Rangarajan A, Hong SJ, Gifford A & Weinberg RA Species- and cell type-specific requirements for cellular transformation. Cancer cell 6, 171–183, doi:10.1016/j.ccr.2004.07.009 (2004). [PubMed: 15324700]
3. Sablina AA, Hector M, Colpaert N & Hahn WC Identification of PP2A complexes and pathways involved in cell transformation. Cancer research 70, 10474–10484, doi: 10.1158/0008-5472.can-10-2855 (2010). [PubMed: 21159657]
4. Sablina AA et al. The tumor suppressor PP2A Abeta regulates the RalA GTPase. Cell 129, 969–982, doi:10.1016/j.cell.2007.03.047 (2007). [PubMed: 17540176]
5. Chen W et al. Identification of specific PP2A complexes involved in human cell transformation. Cancer cell 5, 127–136 (2004). [PubMed: 14998489]
6. Sangodkar J et al. Activation of tumor suppressor protein PP2A inhibits KRAS-driven tumor growth. The Journal of clinical investigation 127, 2081–2090, doi:10.1172/jci89548 (2017). [PubMed: 28504649]
7. Kauko O et al. PP2A inhibition is a druggable MEK inhibitor resistance mechanism in KRAS-mutant lung cancer cells. Science translational medicine 10, doi:10.1126/scitranslmed.aaq1093 (2018).
8. Seshacharyulu P, Pandey P, Datta K & Batra SK Phosphatase: PP2A structural importance, regulation and its aberrant expression in cancer. Cancer letters 335, 9–18, doi:10.1016/j.canlet. 2013.02.036 (2013). [PubMed: 23454242]
9. Shi Y Serine/threonine phosphatases: mechanism through structure. Cell 139, 468–484, doi: 10.1016/j.cell.2009.10.006 (2009). [PubMed: 19879837]
10. Sangodkar J et al. All roads lead to PP2A: exploiting the therapeutic potential of this phosphatase. The FEBS journal 283, 1004–1024, doi:10.1111/febs.13573 (2016). [PubMed: 26507691]
11. Zhou J, Pham HT, Ruediger R & Walter G Characterization of the Aalpha and Abeta subunit isoforms of protein phosphatase 2A: differences in expression, subunit interaction, and evolution. The Biochemical journal 369, 387–398, doi:10.1042/bj20021244 (2003). [PubMed: 12370081]
12. Groves MR, Hanlon N, Turowski P, Hemmings BA & Barford D The structure of the protein phosphatase 2A PR65/A subunit reveals the conformation of its 15 tandemly repeated HEAT motifs. Cell 96, 99–110 (1999). [PubMed: 9989501]
13. Calin GA et al. Low frequency of alterations of the alpha (PPP2R1A) and beta (PPP2R1B) isoforms of the subunit A of the serine-threonine phosphatase 2A in human neoplasms. Oncogene 19, 1191–1195, doi:10.1038/sj.onc.1203389 (2000). [PubMed: 10713707]
14. Shih Ie M et al. Somatic mutations of PPP2R1A in ovarian and uterine carcinomas. The American journal of pathology 178, 1442–1447, doi:10.1016/j.ajpath.2011.01.009 (2011). [PubMed: 21435433]

15. Ruediger R, Pham HT & Walter G Alterations in protein phosphatase 2A subunit interaction in human carcinomas of the lung and colon with mutations in the A beta subunit gene. Oncogene 20, 1892–1899, doi:10.1038/sj.onc.1204279 (2001). [PubMed: 11313937]
16. Haesen D et al. Recurrent PPP2R1A Mutations in Uterine Cancer Act through a Dominant-Negative Mechanism to Promote Malignant Cell Growth. Cancer research 76, 5719–5731, doi: 10.1158/0008-5472.Can-15-3342 (2016). [PubMed: 27485451]
17. Chen W, Arroyo JD, Timmons JC, Possemato R & Hahn WC Cancer-associated PP2A Aalpha subunits induce functional haploinsufficiency and tumorigenicity. Cancer research 65, 8183–8192, doi:10.1158/0008-5472.Can-05-1103 (2005). [PubMed: 16166293]
18. Walter G & Ruediger R Mouse model for probing tumor suppressor activity of protein phosphatase 2A in diverse signaling pathways. Cell cycle (Georgetown, Tex.) 11, 451–459, doi:10.4161/cc.11.3.19057 (2012).
19. Ruediger R, Ruiz J & Walter G Human cancer-associated mutations in the Aalpha subunit of protein phosphatase 2A increase lung cancer incidence in Aalpha knock-in and knockout mice. Molecular and cellular biology 31, 3832–3844, doi:10.1128/mcb.05744-11 (2011). [PubMed: 21791616]
20. Jeong AL et al. Patient derived mutation W257G of PPP2R1A enhances cancer cell migration through SRC-JNK-c-Jun pathway. Scientific reports 6, 27391, doi:10.1038/srep27391 (2016). [PubMed: 27272709]
21. Junk DJ, Cipriano R, Bryson BL, Gilmore HL & Jackson MW Tumor microenvironmental signaling elicits epithelial-mesenchymal plasticity through cooperation with transforming genetic events. Neoplasia (New York, N.Y.) 15, 1100–1109 (2013).
22. Garbe JC et al. Molecular distinctions between stasis and telomere attrition senescence barriers shown by long-term culture of normal human mammary epithelial cells. Cancer research 69, 7557–7568, doi:10.1158/0008-5472.can-09-0270 (2009). [PubMed: 19773443]
23. Cipriano R et al. TGF-beta signaling engages an ATM-CHK2-p53-independent RAS-induced senescence and prevents malignant transformation in human mammary epithelial cells. Proc Natl Acad Sci U S A 108, 8668–8673, doi:10.1073/pnas.1015022108 (2011). [PubMed: 21555587]
24. Wiemann S, P. C., Hu Y, Hunter P, Harbers M, Amiet A, Bethel G, Busse M, Carninci P, Dunham I, Hao T, Harper JW, Hayashizaki Y, Heil O, Hennig S, Hotz-Wagenblatt A, Jang W, Jöcker A, Kawai J, Koenig C, Korn B, Lambert C, LeBeau A, Lu S, Maurer J, Moore T, Ohara O, Park J, Rolfs A, Salehi-Ashtiani K, Seiler C, Simmons B, van Brabant Smith A, Steel J, Wagner L, Weaver T, Wellenreuther R, Yang S, Vidal M, Gerhard DS, LaBaer J, Temple G, Hill DE. The ORFeome Collaboration: a genome-scale human ORF-clone resource. Nature methods 13, 191–192, doi:10.1038/nmeth.3776 (2016). [PubMed: 26914201]
25. Schlatzer D et al. A Targeted Mass Spectrometry Assay for Detection of HIV Gag Protein Following Induction of Latent Viral Reservoirs. Analytical chemistry 89, 5325–5332, doi:10.1021/acs.analchem.6b05070 (2017). [PubMed: 28467046]
26. Mellacheruvu D et al. The CRAPome: a contaminant repository for affinity purification-mass spectrometry data. Nature methods 10, 730–736, doi:10.1038/nmeth.2557 (2013). [PubMed: 23921808]
27. Morris JH et al. Affinity purification-mass spectrometry and network analysis to understand protein-protein interactions. Nature protocols 9, 2539–2554, doi:10.1038/nprot.2014.164 (2014). [PubMed: 25275790]
28. Knight JDR et al. ProHits-viz: a suite of web tools for visualizing interaction proteomics data. Nature methods 14, 645–646, doi:10.1038/nmeth.4330 (2017). [PubMed: 28661499]
29. Wisniewski JR, Zougman A, Nagaraj N & Mann M Universal sample preparation method for proteome analysis. Nature methods 6, 359–362, doi:10.1038/nmeth.1322 (2009). [PubMed: 19377485]
30. McClinch K et al. Small-Molecule Activators of Protein Phosphatase 2A for the Treatment of Castration-Resistant Prostate Cancer. Cancer research 78, 2065–2080, doi: 10.1158/0008-5472.can-17-0123 (2018). [PubMed: 29358171]

31. Casado P et al. Kinase-substrate enrichment analysis provides insights into the heterogeneity of signaling pathway activation in leukemia cells. Science signaling 6, rs6, doi:10.1126/scisignal.2003573 (2013). [PubMed: 23532336]
32. Wiredja DD, Koyuturk M & Chance MR The KSEA App: a web-based tool for kinase activity inference from quantitative phosphoproteomics. Bioinformatics (Oxford, England), doi:10.1093/bioinformatics/btx415 (2017).
33. Fabregat A et al. The Reactome pathway Knowledgebase. Nucleic acids research 44, D481–487, doi:10.1093/nar/gkv1351 (2016). [PubMed: 26656494]
34. Abagyan R, Totrov M & Kuznetsov D ICM- A new method for protein modeling and design: Applicataions to docking and structure prediction from the distorted native conformation. Journal of computational chemistry 15, 488–506 (1994).
35. Doerr S, Harvey MJ, Noe F & De Fabritiis G HTMD: High-Throughput Molecular Dynamics for Molecular Discovery. Journal of chemical theory and computation 12, 1845–1852, doi:10.1021/acs.jctc.6b00049 (2016). [PubMed: 26949976]
36. Case DA et al. The Amber biomolecular simulation programs. Journal of computational chemistry 26, 1668–1688, doi:10.1002/jcc.20290 (2005). [PubMed: 16200636]
37. Price DJ & Brooks CL 3rd. A modified TIP3P water potential for simulation with Ewald summation. The Journal of chemical physics 121, 10096–10103, doi:10.1063/1.1808117 (2004). [PubMed: 15549884]
38. Berendsen HJC, Postma JPM, Gunsteren W. F. v., DiNola A & Haak JR Molecular dynamics with coupling to an external bath. The Journal of chemical physics 81, doi:1.448118 (1984).
39. Harvey MJ, Giupponi G & Fabritiis GD ACEMD: Accelerating Biomolecular Dynamics in the Microsecond Time Scale. Journal of chemical theory and computation 5, 1632–1639, doi:10.1021/ct9000685 (2009). [PubMed: 26609855]
40. Bonomi M, Barducci A & Parrinello M Reconstructing the equilibrium Boltzmann distribution from well-tempered metadynamics. Journal of computational chemistry 30, 1615–1621, doi:10.1002/jcc.21305 (2009). [PubMed: 19421997]
41. Skliros A et al. The importance of slow motions for protein functional loops. Physical biology 9, 014001, doi:10.1088/1478-3975/9/1/014001 (2012). [PubMed: 22314977]
42. Hess B, Kutzner C, van der Spoel D & Lindahl E GROMACS 4: Algorithms for Highly Efficient, Load-Balanced, and Scalable Molecular Simulation. Journal of chemical theory and computation 4, 435–447, doi:10.1021/ct700301q (2008). [PubMed: 26620784]
43. DeLano W PyMOL molecular viewer: Updates and refinements. Abstracts of Papers of the American Chemical Society 238 (2009).
44. Humphrey W, Dalke A & Schulten K VMD: visual molecular dynamics. Journal of molecular graphics 14, 33–38, 27-38 (1996). [PubMed: 8744570]
45. Kamburov A et al. Comprehensive assessment of cancer missense mutation clustering in protein structures. Proc Natl Acad Sci U S A 112, E5486–5495, doi:10.1073/pnas.1516373112 (2015). [PubMed: 26392535]
46. Rahman M et al. PPP2R1A mutation is a rare event in ovarian carcinoma across histological subtypes. Anticancer research 33, 113–118 (2013). [PubMed: 23267135]
47. Hoang LN et al. Targeted mutation analysis of endometrial clear cell carcinoma. Histopathology 66, 664–674, doi:10.1111/his.12581 (2015). [PubMed: 25308272]
48. Jones S et al. Frequent mutations of chromatin remodeling gene ARID1A in ovarian clear cell carcinoma. Science (New York, N.Y.) 330, 228–231, doi:10.1126/science.1196333 (2010).
49. Pallas DC et al. Polyoma small and middle T antigens and SV40 small t antigen form stable complexes with protein phosphatase 2A. Cell 60, 167–176 (1990). [PubMed: 2153055]
50. O'Connor CM, Hoffa MT, Taylor SE, Avelar RA & Narla G Protein phosphatase 2A Aalpha regulates Abeta protein expression and stability. The Journal of biological chemistry, doi:10.1074/jbc.RA119.007593 (2019).
51. Taylor SE et al. The highly recurrent PP2A Aalpha-subunit mutation P179R alters protein structure and impairs PP2A enzyme function to promote endometrial tumorigenesis. Cancer research, doi:10.1158/0008-5472.can-19-0218 (2019).

52. Strack S, Cribbs JT & Gomez L Critical role for protein phosphatase 2A heterotrimers in mammalian cell survival. The Journal of biological chemistry 279, 47732–47739, doi:10.1074/jbc.M408015200 (2004). [PubMed: 15364932]

53. Letourneux C, Rocher G & Porteu F in EMBO J Vol. 25 727–738 (2006). [PubMed: 16456541]

54. Horn T et al. Mapping of signaling networks through synthetic genetic interaction analysis by RNAi. Nature methods 8, 341–346, doi:10.1038/nmeth.1581 (2011). [PubMed: 21378980]

55. Holt SV et al. Enhanced apoptosis and tumor growth suppression elicited by combination of MEK (selumetinib) and mTOR kinase inhibitors (AZD8055). Cancer research 72, 1804–1813, doi:10.1158/0008-5472.can-11-1780 (2012). [PubMed: 22271687]

56. Roberts PJ et al. Combined PI3K/mTOR and MEK inhibition provides broad antitumor activity in faithful murine cancer models. Clinical cancer research : an official journal of the American Association for Cancer Research 18, 5290–5303, doi:10.1158/1078-0432.ccr-12-0563 (2012). [PubMed: 22872574]

57. Grinthal A, Adamovic I, Weiner B, Karplus M & Kleckner N PR65, the HEAT-repeat scaffold of phosphatase PP2A, is an elastic connector that links force and catalysis. Proc Natl Acad Sci U S A 107, 2467–2472, doi:10.1073/pnas.0914073107 (2010). [PubMed: 20133745]

58. Tsytlonok M et al. Complex energy landscape of a giant repeat protein. Structure (London, England : 1993) 21, 1954–1965, doi:10.1016/j.str.2013.08.028 (2013).

59. Caunt CJ, Sale MJ, Smith PD & Cook SJ MEK1 and MEK2 inhibitors and cancer therapy: the long and winding road. Nature reviews. Cancer 15, 577–592, doi:10.1038/nrc4000 (2015). [PubMed: 26399658]

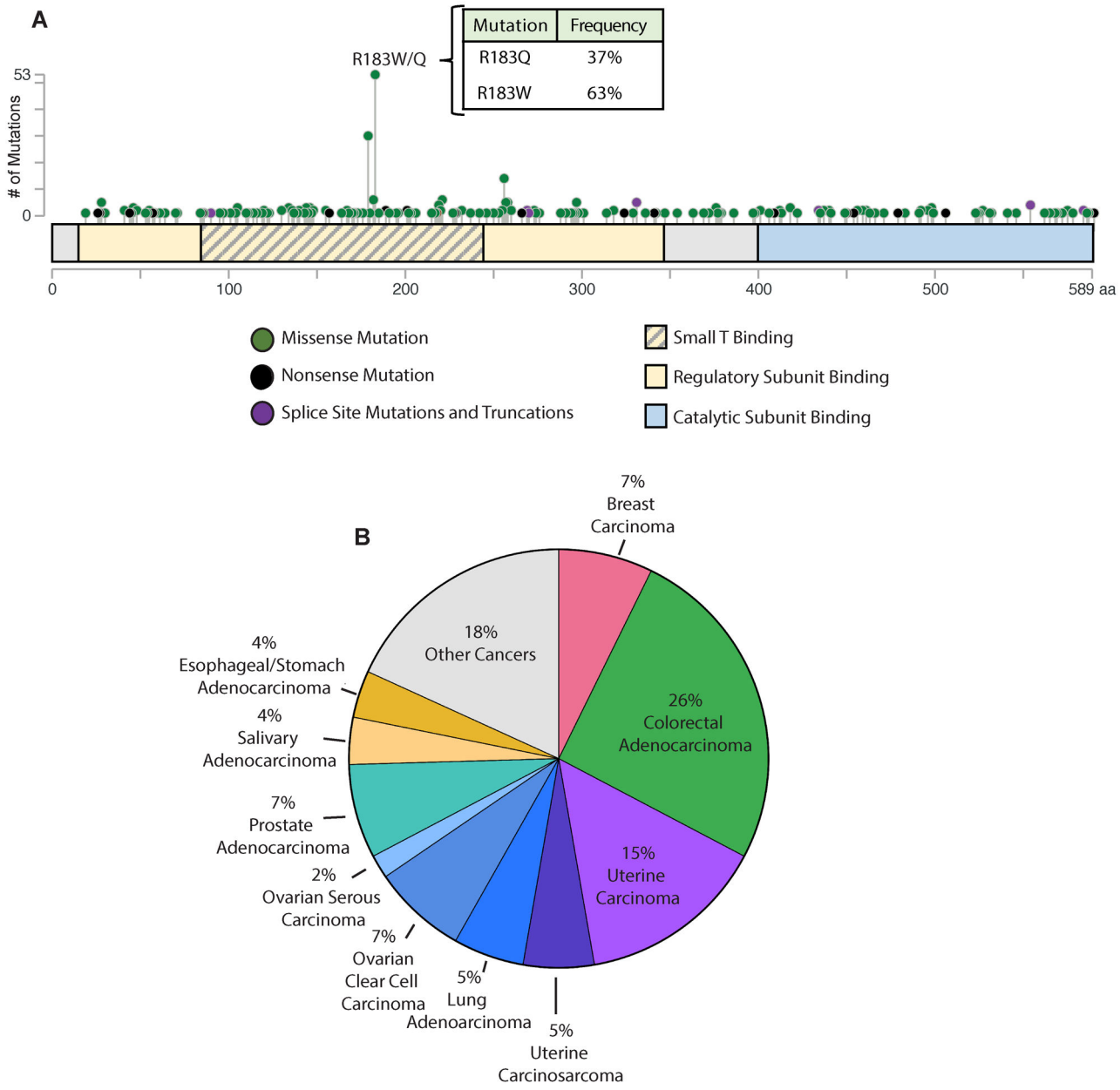

Figure 1. R183W is the most commonly mutated residue of PP2A Aα across human cancer.

(**A**) Representation of all identified heterozygous missense mutations to the Aα subunit distributed across the length of the protein. The y-axis shows the number of mutations and the type of mutations are represented by colored dots. Green dots indicate missense mutations, black dots indicate nonsense mutations, and purple dots indicate splice site mutations and truncations (adapted from cBioportal.org). Binding regions relevant to Aα are indicated by the colored boxes. Yellow indicates regulatory subunit binding regions, yellow with grey lines indicate the region within the regulatory subunit binding region where SV40 small T antigen binds, and blue indicates the catalyic subunit binding region. (**B**) The distribution of all heterozygous missense mutations to the R183 residue by histological subtype.

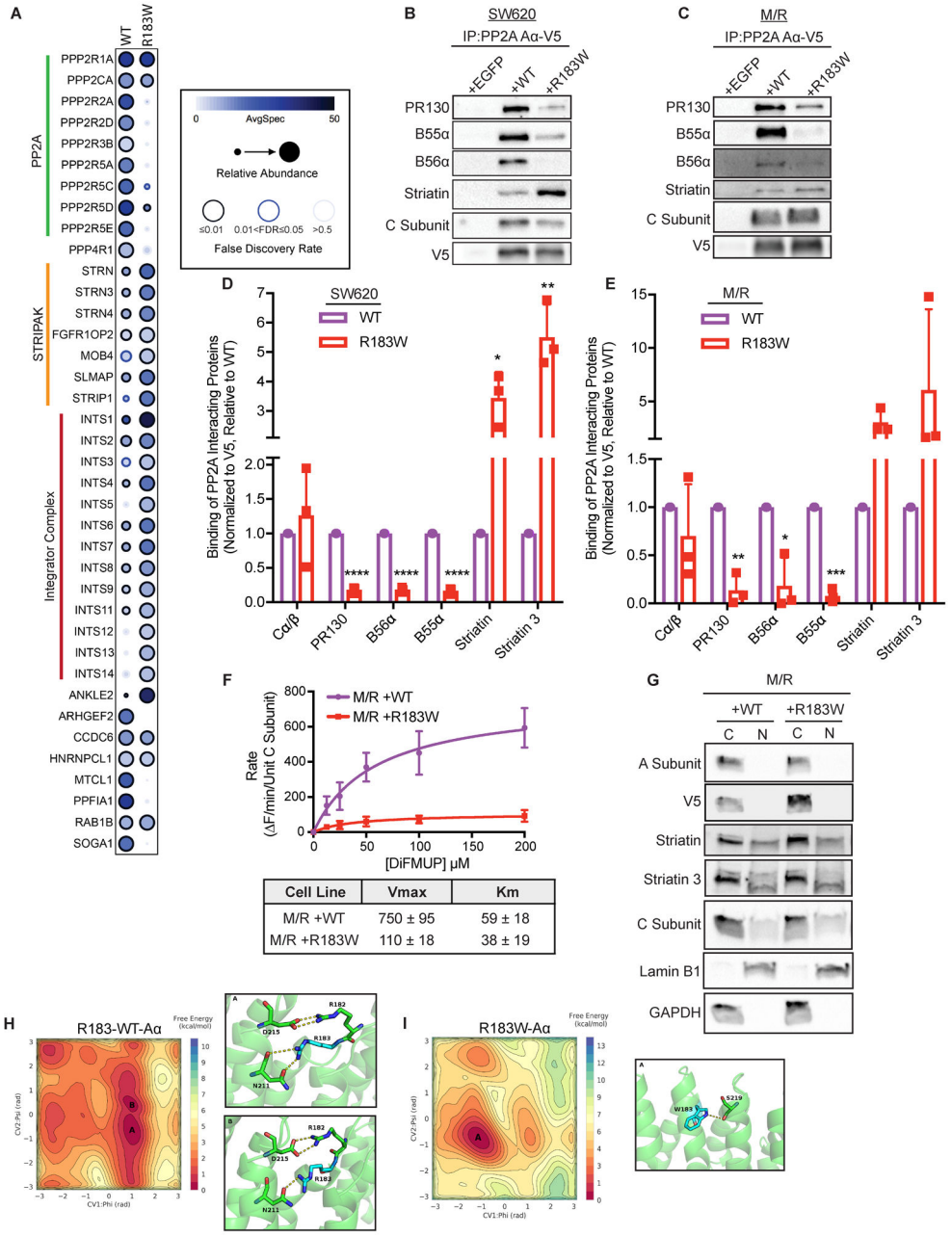

Figure 2. Aα R183W alters the PP2A interactome and decreases PP2A activity.

(**A**) AP-MS analysis of V5 tagged wild type or R183W Aα protein from SW620 cells. Data is represented as a dot plot: the color of the circle indicates the spectral count values, circle size displays the relative abundance of preys (interacting proteins) between baits (WT and R183W mutant Aα protein, finally, the colored edge of the circles indicates the FDR or confidence of the interaction. Statistical analysis performed by SAINT and visualization performed using ProHits-viz (n=3). (**B and C**) Co-immunoprecipitation of V5-tagged wild type or R183W Aα protein to determine binding of select PP2A family members from SW620 cells (**B**) and M/R cells (**C**). **(D and E)** Quantification of relative binding of PP2A subunit family members from co-immunoprecipitation of V5-tagged wild type or R183W

Aα protein in SW620 (D) or M/R (E) cells. Binding normalized to V5 levels and plotted relative to wild type Aα, n=3 (Multiple T-tests, with Holm-Sidak method of correction for multiple comparisons: p-values: *<0.05, **≤0.01, ***≤0.001, ****≤0.0001). (**F**) PP2A activity assay of WT (purple) and mutant R183W (red) Aα holoenzymes. Briefly, V5-tagged WT and R183W Aα protein was co-immunoprecipitated and the resulting IPs, including co-immunopreciptated proteins, were incubated for 15 minutes with increasing concentrations of DiFMUP and analyzed for activity by fluorescence, data presented as the mean ± SD (n=3). **(G)** Immunoblot analysis of select PP2A subunits from cytoplasmic and nuclear fractionation of cell lysates from M/R cells expressing V5-tagged wild type or R183W Aα protein, showing that localization of the mutant protein and subsequent subunits is unchanged relative to wild type. A representative immunoblot is shown, (n=3). (**H**) Free energy surface (FES) plot of the WT Aα subunit, as calculated from Well Tempered-metadynamics simulations. The two minima have been labelled as A and B. The representative structure of the clustered conformations in the minima has been illustrated. In the minimum, the side chain of R183 makes interactions with the side chain of N211. This interaction is facilitated by an ion pair interaction between R182 and D215. **(I)** Free energy surface (FES) plot of the R183W mutant Aα subunit, as calculated from Well Tempered-metadynamics simulations. The deepest minimum has been labelled as A. The representative structure of the clustered conformations in the minima has been illustrated. In the minimum, the side chain of R183W mutant makes interactions with the backbone carbonyl oxygen atom of S219. The loss of interactions as a result of the mutation pushes the A subunit into a conformation that is not observed in the WT R183 PP2A Aα subunit.

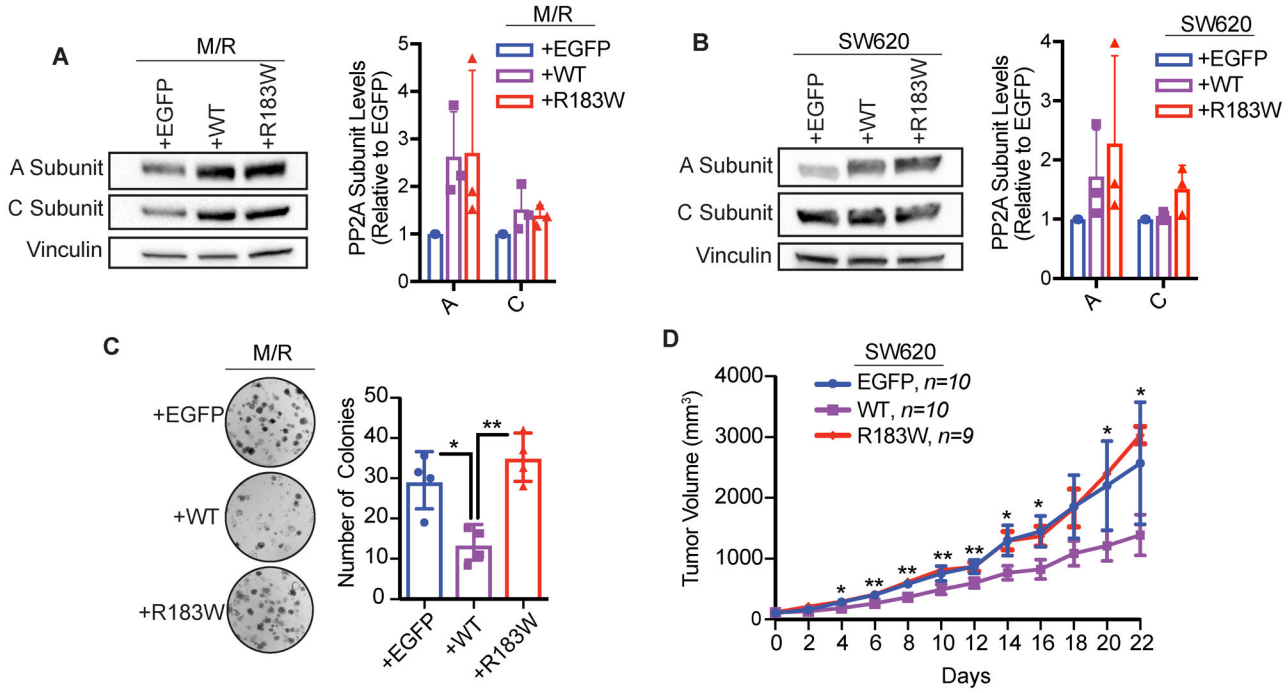

Figure 3. The R183W mutation loses growth suppressive activity compared to wild type PP2A.

(**A**) Western blot validation of A and C subunit expression levels from M/R stable cell lines and quantification, data presented as mean ± SD (n=3). **B**) Western blot validation of A and C subunit expression levels from SW620 stable cell lines and quantification, data presented as mean ± SD (n=3). (**C**) Clonogenic assay of M/R cells, briefly, 500 cells were seeded in 6 well plates and allowed to grow for 10 days, then fixed, stained with crystal violet, and quantified via ImageJ. Three technical replicates per biological replicate, data represented as the mean ± SD (n=4). (One-way ANOVA; Tukey's correction for multiple comparisons, p-values: *<0.05, **≤0.01). (**D**) Xenograft assay of SW620 cells expressing EGFP (control vector) (n=10), wild type Aα (n=10) or Aα-R183W (n=9), injected subcutaneously into the flanks of female nude mice. Tumors were measured every other day. Data are presented as mean ± SEM (Students T-tests, R183W relative to WT, p-values: * < 0.05, ** ≤ 0.01).

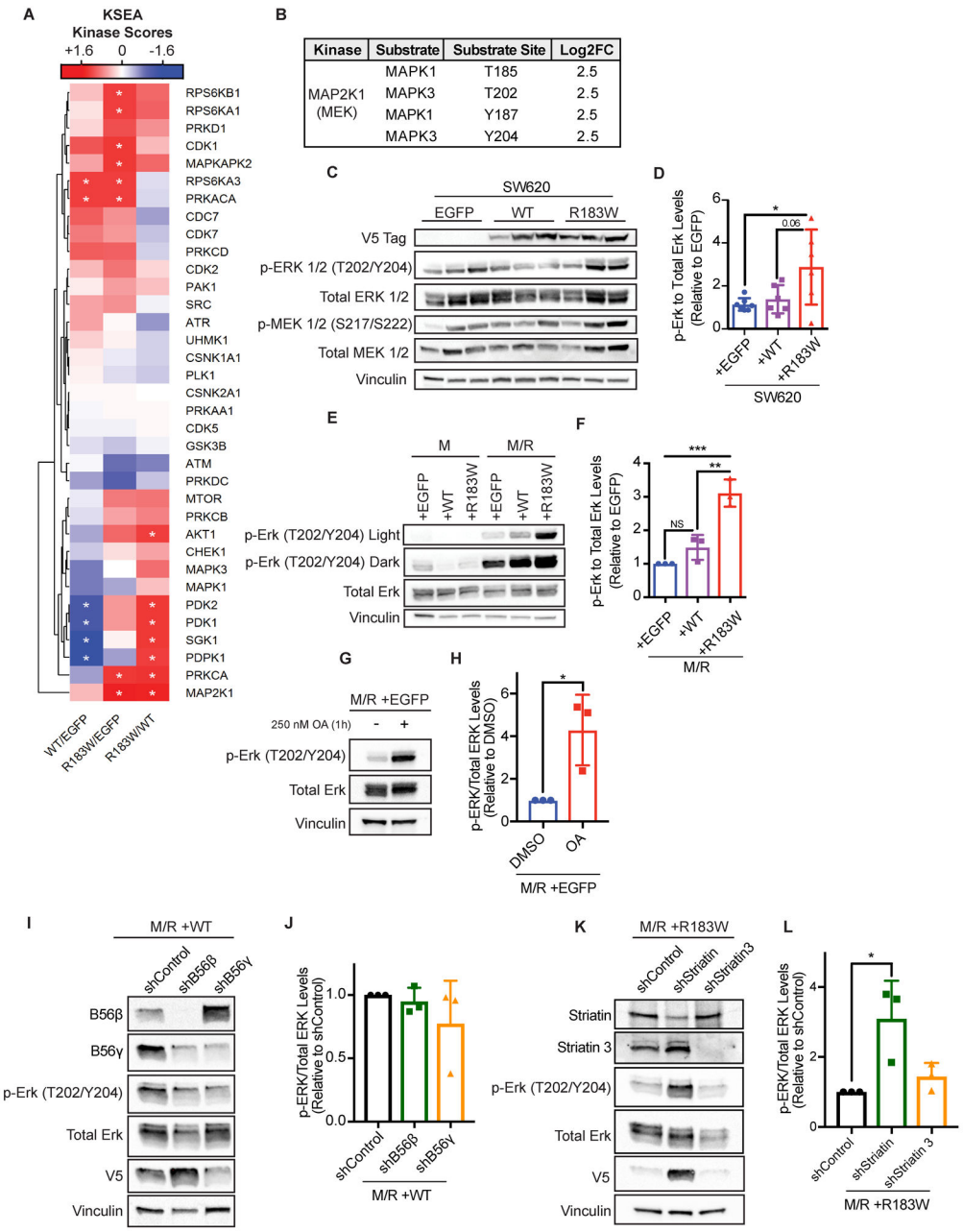

Figure 4. Aα-R183W expression alters the phosphoproteome and increases MAPK signaling.

(**A**) Three tumors from each group of the SW620 xenograft were analyzed for global serine/threonine phosphoproteomics. Kinase-Substrate Enrichment Analysis (KSEA) was performed on the phosphoproteomic dataset to estimate relative changes in kinase activity. The normalized kinase scores are color coded in the heat map; blue = negative score. meaning a decrease in kinase activity in the experimental group (numerator of the fold change) relative to the reference group (denominator). Inversely, red = positive score, which is an increase in kinase activity in the experimental group (numerator) relative to the reference (denominator). White = zero, no change between the groups (Asterisks mark the scores with p-value < 0.05, as calculated by a z-test. Only kinases with at least 3 identified

substrates are illustrated). (**B**) Table showing identified phosphorylated substrates and phosphosites of MAP2K1 from the KSEA analysis. (**C**) Western blot validation and quantification of phosphorylated and total ERK and MEK levels in SW620 tumors. (**D**) Quantification of phospho-ERK relative to total ERK in cohort of SW620 tumors expressing EGFP, Aα WT, and Aα R183W. Ratio of phospho/total levels is plotted relative to one EGFP tumor, data are presented as mean ± SD, (One-way ANOVA; Tukey's correction for multiple comparisons, p-values: * < 0.05, ** ≤ 0.01). (**E**) Representative western blot of p-ERK and total ERK in HMEC cells. **(F)** Quantification of phospho-ERK relative to total ERK from M/R-WT and M/R-R183W cells, data presented as mean ± SD (Right) (n=3) (One-way ANOVA; Tukey's correction for multiple comparisons, p-values: ** ≤ 0.01, *** ≤ 0.001). (**G**) Representative western blot of p-ERK and total ERK in M/R +EGFP cells treated with 250 nM okadaic acid (OA) for 1 hour. (**H**) Quantification of p-ERK relative to total ERK from the M/R +EGFP cells, data presented as mean ± SD (n=3) (Unpaired t-test, p-values: * < 0.05). (**I**) Representative western blot of p-ERK and total ERK in M/R +WT cells treated with shControl, shB56β, or shB56γ lentivirus for 72 hours. Quantification of shB56β and shB56γ knockdown in Supplemental Figure X. (**J**) Quantification of p-ERK relative to total ERK from the M/R +WT cells, data presented as mean ± SD (n=3) (One-way ANOVA; Dunnett's correction for multiple comparisons, no significant values). (**K**) Representative western blot of p-ERK and total ERK in M/R +R183W cells treated with shControl, shStriatin, or shStriatin 3 lentivirus for 72 hours. Quantification of shStriatin and shStriatin 3 knockdown in Supplemental Figure X. (**L**) Quantification of p-ERK relative to total ERK from the M/R +R183W cells, data presented as mean ± SD (n=3) (One-way ANOVA; Dunnett's correction for multiple comparisons, p-values: * < 0.05).

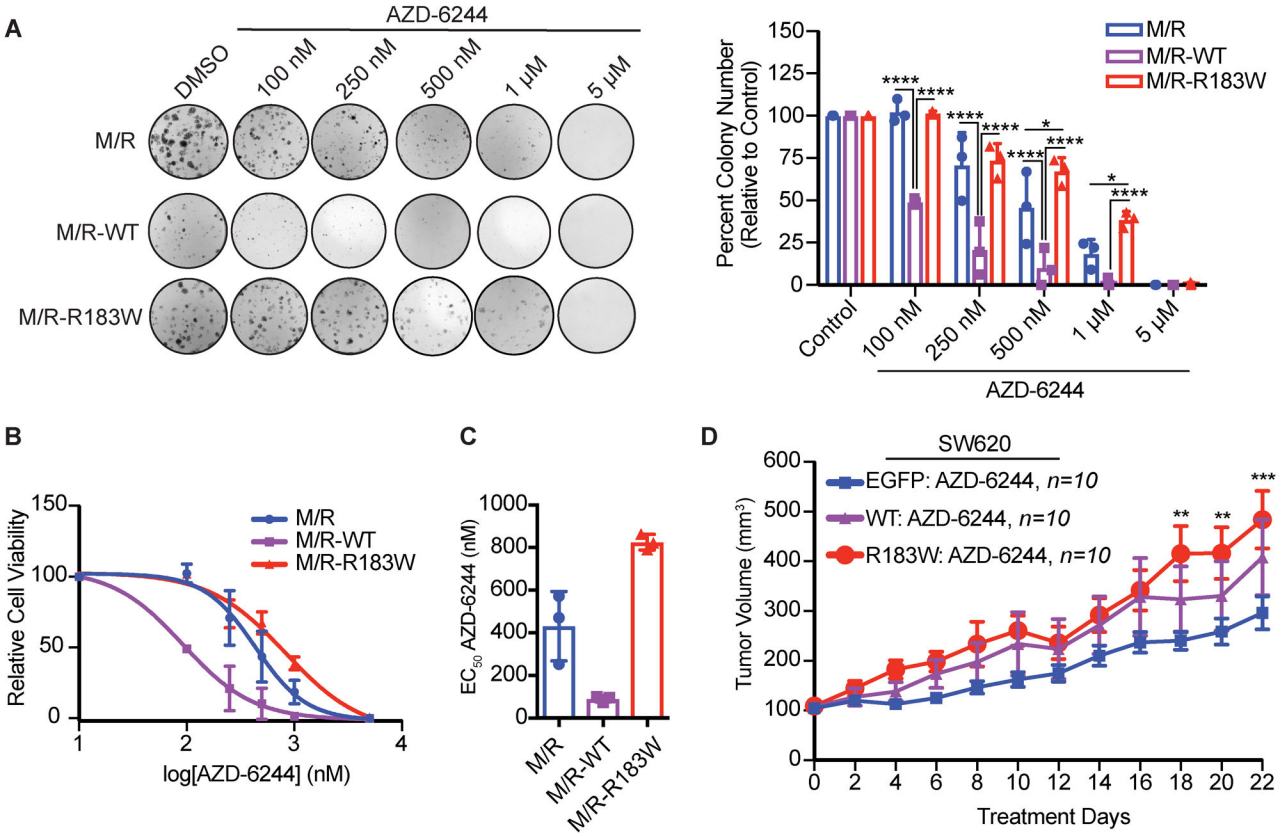

Figure 5. Expression of R183W decreases sensitivity to MEK Inhibition.

(**A**) Clonogenic assay of M/R cells expressing WT or R183W Aα protein. Cells were seeded at 500 cells/well, 24hr after seeding cells were treated with vehicle control or increasing concentrations of AZD-6244 and allowed to grow for 10 days. Cells were fixed and stained with crystal violet and quantified using ImageJ. The graph represents the mean colony number ± SD relative to the vehicle control. Three technical replicates per biological replicate (n=3). (2-Way ANOVA, with Tukey's correction for multiple comparisons, p-values: * < 0.05, **** ≤ 0.0001). (**B**) Representation of the clonogenic assay as a log dose-response curve, data represented as mean ± SD (n=3). **(C)** Corresponding graph of the calculated EC_{50} values for each of the cell lines, data represented as mean ± SD (n=3). (**D**) 5×10^6 SW620 cells expressing WT or R183W Aα protein or EGFP control vector were injected subcutaneously in nude mice (n=10 per group) and allowed to grow to 100 mm^3, randomized and treated with 25 mg/kg AZD-6244 BID for 22 days. Graph represents the mean tumor volume ± SEM, (2-Way ANOVA, with Tukey's correction for multiple comparisons, p-values: ** ≤ 0.01, *** ≤ 0.001, EGFP vs. R183W).